Scale, scaling and multifractals in geophysics: twenty years on

Shaun Lovejoy[1] and Daniel Schertzer[2]

[1]Physics, McGill University, 3600 University st., Montreal, Que. H3A 2T8, Canada, lovejoy@physics.mcgill.ca

[2] CEREVE, Ecole Nationale des Ponts et Chaussées,6-8, avenue Blaise Pascal, Cité Descartes, 77455 MARNE-LA-VALLEE Cedex, France, Daniel.Schertzer@enpc.fr

Abstract.
We consider three developments in high number of degrees of freedom approaches to nonlinear geophysics: a) the transition from fractal geometry to multifractal processes, b) the self-organized critical (SOC) generation of extremes via classical and nonclassical (multifractal) SOC, c) the generalization from isotropic scale invariance (self-similar fractals, multifractals) to (anisotropic) generalized scale invariance. We argue that these innovations are generally necessary for geophysical applications. We illustrate these ideas with data analyses from both the atmosphere and the earth's surface, as well as with multifractal simulations.

1. Introduction: Which Chaos for geophysics?

During the 1960's, 70's and 80's developments in physics and mathematics spawned three related nonlinear geophysics paradigms. The first, deterministic chaos, was centred around the discovery [*Lorenz*, 1963] that systems with as few as three degrees of freedom could have random-like "chaotic" behaviour. The second, fractal geometry - proposed that many natural systems could be modeled as (stochastic, scale invariant) fractal sets [*Mandelbrot*, 1967]. The third, "self-organized criticality" (SOC) [*Bak, et al.*, 1987] proposed that extreme events could be the result of seemingly simple generic avalanche-like processes. By the early 1980's further developments had made the first two quite practical. In particular, the discovery of universality in chaos by [*Feigenbaum*, 1978] had made it possible to make chaotic models of real world systems, and the revolution in computer graphics had made fractals – including "strange" chaotic attractors – palpable.

This short expose gives an overview of certain subsequent developments covering roughly the twenty years celebrated by the conference. While deterministic chaos is essentially a low degrees of freedom paradigm, fractals and SOC are both high number of degrees of freedom frameworks and could

thus be called "stochastic chaos" since they involve infinite dimensional probability spaces [*Lovejoy and Schertzer*, 1998a]. While the question of whether deterministic or stochastic chaos is more geophysically relevant continues to be debated [*Schertzer, et al.*, 2002], here we focus on the latter. We outline three key developments which allow the fractal and SOC paradigms to be widely applicable in geosciences: a) the transition from scale invariant sets (fractals) to scale invariant fields (multifractals), b) the recognition of the link between extreme events, heavy tailed (algebraic) probabilities (SOC) and space-time scaling, c) the generalization of scale invariance from isotropic (self-similar) systems to very general anisotropic ones (self-affine and beyond) within the framework of Generalized Scale Invariance (GSI). Rather than attempt a systematic survey, we illustrate our discussion using results from key fields in solid earth and atmospheric geophysics: the earth's topography and clouds and rain. This choice is motivated by both the fundamental significance of the fields and for the availability of relevant high quality data.

2. The link between descriptions and models:

It is an old truism that one cannot make a measurement without first having a theory of what is to be measured. This is well illustrated in nonlinear geophysics where theoretical developments are not only necessary for making more sophisticated theories and better applications: they are necessary simply in order to quantitatively *describe* geofields. We illustrate this statement with two significant examples. The first is the long debate starting in the 1980's about what was the (supposedly unique) fractal dimension of the earth's topography. If the topography could be adequately modeled as a geometrical fractal set, then many different techniques (including spectral analysis) could be used to estimate its unique dimension D. Unfortunately, different techniques applied to different data commonly gave different values of D (see the review in [*Klinkenberg and Goodchild*, 1992]). Consequently by the end of the 1990's the mainstream surface geomorphology community had "moved on", relegating fractals to narrow ranges of scale and to very technical applications. This near abandonment of scaling occurred in spite of the fact that entire fields of research such as surface hydrology (see e.g. the excellent review [*Rodriguez-Iturbe and Rinaldo*, 1997]) are riddled with scaling laws which virtually require the topography to respect some form of scaling. At the same time, due to their random singularities, multifractals have such strong variability that they violate many conventional geostatistical assumptions so that normal multifractal variability can easily be misinterpreted in terms of spurious scale breaks, spurious nonstationarity etc. The loss of interest in scaling was encouraged by the extensive use of (low vari-

ability) fractional Brownian motion (fBm) models of topography. As argued in [*Gagnon, et al*., 2006], the topography in fact has excellent multiscaling (multifractal) properties (see fig. 2, 4, 7) – but an infinite hierarchy of fractal dimensions; this requires new analysis techniques. Consequently the lack of an adequate theoretical framework for scaling has led the baby to be thrown out with the bathwater.

Similarly, in the atmosphere the still dominant model of atmospheric dynamics is of a small scale 3D isotropic turbulence superposed on a large scale 2D isotropic turbulence with the two separated by a "dimensional transition" somewhere near the 10km scale thickness (the "meso-scale gap", [*Van der Hoven*, 1957]). This model is increasingly at odds with modern data – particularly of the vertical structure - which fails to find evidence of any isotropic turbulent regime whatsoever (see [*Lovejoy, et al*., 2006])! Indeed, the mainstream experimentalists espouse anisotropic but scaling gravity wave models (e.g. [*Dewan*, 1997] [*Gardner*, 1994]) which are equivalent to "elliptical dimensions" (see below) D_s=7/3 (in between 2 and 3), whereas high resolution vertical cross data (from lidars) favour a value closer to 23/9 [*Lilley, et al*., 2004]. Today, probably the key element blocking a consensus is the fact that there is still no general agreement about the horizontal structure. This is where a marriage between theory and measurements is required: how to interpret the aircraft data which are our primary source of dynamical (velocity) data in the horizontal? The basic problem is that even aircraft on scientific missions cannot maintain perfectly "flat" trajectories. In a 2D turbulence, the vertical would be smooth and there would be no biases in estimates of spectral exponents. Similarly, in 3D isotropic turbulence, even if the trajectories are non-smooth there is a single exponent (independent of direction), so again the measured exponent can plausibly be taken at face value. However, if the turbulence is anisotropic with different vertical and horizontal exponents – then the aircraft can have fractal trajectories implying long-range correlations between the aircraft position and atmospheric structures, leading to possible biases in the exponents. In addition, even very small mean vertical slopes can lead to statistics being dominated by vertical rather than horizontal exponents. Both of these effects have been found in stratospheric flights which can have both 1.56 dimensional trajectories [*Lovejoy, et al*., 2004], and then at scales > 300km, Bolgiano-Obukhov ($k^{-11/5}$) rather than Kolmogorov spectra ($k^{-5/3}$; k is a wavenumber). This has made it possible for the first time to explain the major aircraft campaigns (GASP [*Nastrom and Gage*, 1983], MOZAIC [*Lindborg and Cho*, 2001]). This set the ground for a clear understanding of the horizontal structure.

3. Wide range scaling

Scale invariance – no matter how theoretically appealing – would not be of general geophysical interest were it not for the basic empirical fact that geofields display wide range scaling. Figs. 1, 2 show spectral analyses of visible cloud radiances covering the range of roughly 1 m to 5000 km, and fig. 2 of topography covering the range 1 m to 20,000 km. In both cases, the spectra are "isotropic" i.e. the squared modulus of the 2D fourier transform has been angle integrated (and in the case of the cloud data, averaged over the available data). In solid earth geophysics it is more usual to angle aver-age the spectrum; in 2D this will reduce the exponent by one. Below we use angle integration since for isotropic processes, the resulting exponents are independent of the dimension of the analysis space. The use of energy spec-tra has the advantage of relying on familiar data analysis techniques which are quite sensitive to breaks in the scaling. The angle integration "washes out" much of the anisotropy and explains why – in spite of highly diverse cloud morphologies – the isotropic spectra (E(k)) can approximately be of the power law form:

$$E(k) \approx k^{-\beta} \tag{1}$$

(k is the modulus of the wavevector $\underline{k}$). The exponents of such power law spectra are scale invariant because they are invariant under the scale change $\underline{k} \to \lambda \underline{k}$ (corresponding in real space to the scale reduction $\underline{x} \to \lambda^{-1}\underline{x}$ where $\underline{r}$ is position vector); the spectra – which keeps its form but which changes by the factor $\lambda^{-\beta}$ - is called "scaling". In physics the term "scaling" is generally reserved for invariance under space-time scale transformations, although occasionally it is also used to describe the tails of algebraic prob-ability distributions, (in this case it refers to scaling in a probability space; see the discussion of SOC below). In the geosciences there is an unfortunate tendency to use "scaling" to denote the general problem of changing from one scale to another even if there are no conserved properties; below we re-serve the term for the more precise physics sense referring to invariant prop-erties under (possibly anisotropic) scale changes.

Geodata are frequently scaling in time as well as space: i.e. in *space-time*. Indeed, geofluids generally have well-defined space-time relations so that structures of a given spatial extent live for a statistically well-defined dura-tion. For example in turbulence – and in the atmosphere – the lifetime of a structure ("eddy") is referred to as the "eddy-turn over time". The lifetime corresponding to structures of planetary extent (the "synoptic maximum", [*Kolesnikov and Monin*, 1965]) is about 2 weeks and is thus the natural time scale separating the weather from the climate; the latter being the result of

evolution over many eddy turn over times, the former over a single turn-over time. We may therefore expect the long time behaviour of the atmosphere to have different scaling properties from the short time behaviour. In fig. 3a, we show a mean temperature surrogate (from the Greenland GRIP core), the O^{18}/O^{16} ratio showing a clear turbulent-like signal going back over 40,000 years (including highly intermittent "Dansgaard events", the sharp high frequency spikes).
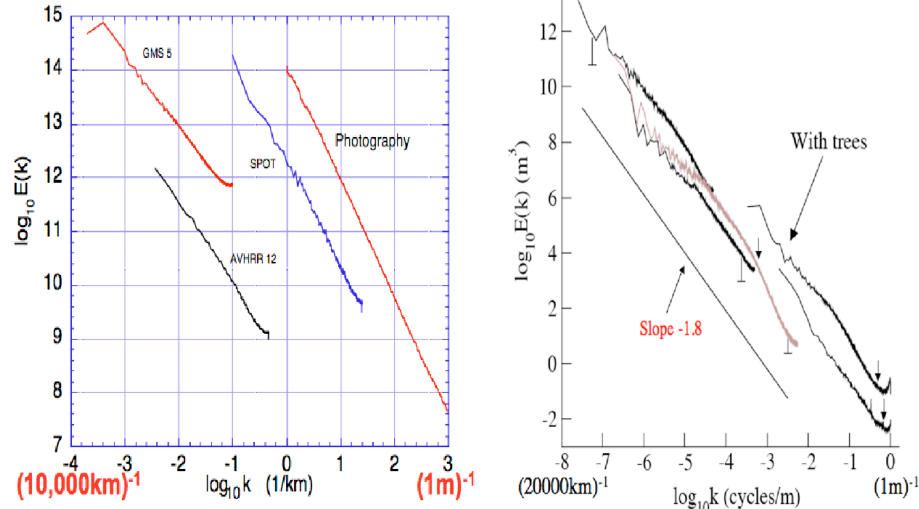

Fig. 1: The average spectra (displaced in the vertical for clarity) obtained for GMS, NOAA 12, data as well as a SPOT image over France. The GMS spectrum shows a range of scales of 5120–10 km, the NOAA 12 spectrum shows a range from 256 to 2 km and the SPOT spectrum shows a range from 10 km to 40 m. At the far right we also show the average of 38 ground based pictures (some with resolutions of 50 cm, this is the average of the data discussed in [Sachs, et al., 2002]). Reproduced from [Lovejoy and Schertzer, 2005].

Fig. 2: Log/log plot of the spectral energy for four Digital Elevation Maps (DEMs). From right to left: Lower Saxony (with trees, top), Lower Saxony (without trees, bottom), the U.S. at 90 m (in grey), at 30" (about 1km, GTOPO30) and the earth (including bathymetry) at 5' (about 10km), ETOPO5. A reference line of slope −2.10 is on the graph to show the overall slope of the spectra. The small arrows show the frequency at which the spectra are not well estimated due to the inadequate dynamical range of the data; see [Gagnon, et al., 2006] for this theoretical estimate (for ETOPO5, it is well estimated over the whole range). The "semi error bar" symbols indicate the amount of offset due to the resolution dependent factor $\lambda^{K(2)}$ (see [Gagnon, et al., 2006] for this necessary resolution dependent correction). Reproduced from [Gagnon, et al., 2006].

Fig. 3b shows that the spectrum is also scaling; with exponent only a little

smaller than for turbulent temperatures ($\beta \approx 1.4$ compared to 5/3). In fact, it seems that the scaling goes back to about 40,000 years [*Lovejoy and Schertzer*, 1986] after which the spectrum flattens out. Note that there is no strong (above background) signal from the precession of the earth's axis so this analysis tends to make the Milankovitch theory for the ice ages less convincing. Since temperature is the basic climate variable, this suggests that scaling is an appropriate framework for modeling and understanding climate.
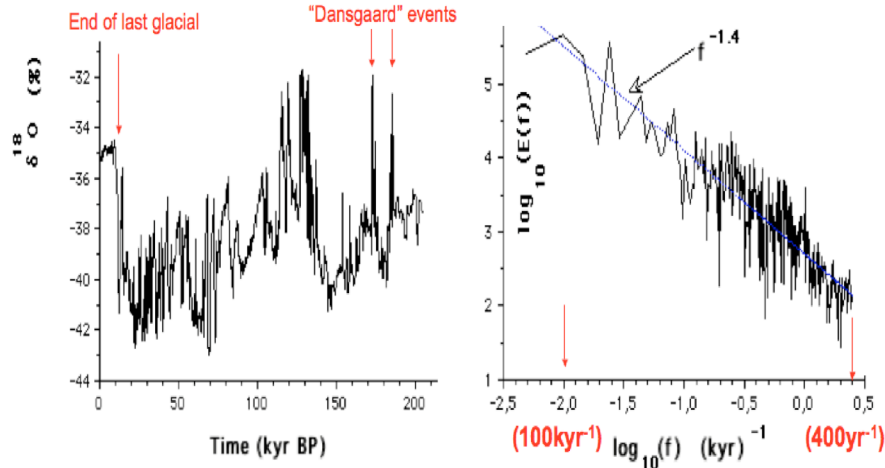

Fig 3a: This figure shows O^{18}/O^{16} in parts per thousand for the Greenland GRIP ice core at 200 year resolution; this is a standard temperature surrogate. The present is at the origin, the past is to the right. Note that the above corresponds to the initial dating of the core; the more modern dating shortens the time scale by nearly a factor of 2 (however, it does not much affect the scaling exponents, F. Schmitt private communication). The "Dansgaard events" are the equivalent of going in and out of an ice age in perhaps as little as 100 years. Adapted from [*Schmitt, et al.*, 1995].	Fig 3b: The spectrum $E(f)$ of the temperature surrogate (fig 3a), with reference slope $f^{1.4}$, this is only a little less steep than the $f^{-5/3}$ spectrum observed in the atmosphere at weather scales (f is the frequency). Adapted from [*Schmitt, et al.*, 1995].

4. From monofractal sets to multifractal fields

Using fourier spectra, we have seen that the basic atmospheric and earth surface fields display wide range scaling in space and time. Spectra were first widely used to characterize turbulence, and in the early 1970's in conjunction with the development of quasi-gaussian statistical closure models,

the theoretical or empirical determination of the spectral exponent became a key task. In quasi-gaussian processes (essentially the "fractional Brownian motions" generalizations of Brownian motion), there is a single basic exponent hence the spectral exponent is simply related to the (unique) fractal dimension of exceedence sets (the set of points exceeding a fixed threshold). However, by the early 1980's, the development of cascade models to study turbulent intermittency lead to the realization that in general an infinite number of dimensions were needed, in fact, the generic result of a cascade process is that the cascade quantity at resolution ε_λ has the statistics:

$$\left\langle \varepsilon_\lambda^q \right\rangle = \lambda^{K(q)} \tag{2}$$

where $K(q)$ is (convex) the moment scaling function and λ is the ratio of the largest (outer) cascade scale and the scale of observation. The symbol "ε" is used for the turbulent (scale by scale) energy flux.

Viewed from the point of multifractals, spectra are second order statistics (for statistically stationary processes, they are the fourier transforms of the autocorrelation functions; the Wiener-Khintchin theorem), so that the spectrum is only a very partial description of its properties. A more complete and direct description follows from the use of thresholds (T) to convert fields $\varepsilon(\underline{x})$ into exceedence sets ($\underline{x}$ is a position vector), and then the use of box-counting to systematically degrade the resolution of the sets, determining the fractal dimension using the formula:

$$N_T(L) \propto L^{-D(T)}; \quad P_T(L) \approx N_T(L)/L^{-d} \approx L^{c(T)}; \quad c(T) = d - D(T) \tag{3}$$

where $N_T(L)$ is the number of LXL sized boxes needed to cover the set of points satisfying $\varepsilon(\underline{x}) > T$. Since L^d is the total number of boxes in the space at resolution L, P_T is the probability that a box (size L) placed at random on the set will cover part of the set. $D(T)$ is the dimension and $c(T)$ is the codimension function which is thus a probability exponent. Since probability exponents can be defined without reference to the embedding space of the process (i.e. whether it occurs in a 1-D, 2-D… or for stochastic processes, in infinite D probability spaces), codimensions are generally needed for stochastic fractals and multifractals.

When this "functional" box-counting was done for the topography (fig. 4) or radar reflectivities of rain (fig. 5), it was found that the scaling was excellent: the power law eq. 3 was accurately obeyed for all T, L. However $D(T)$ systematically decreases with threshold, it is not constant as assumed in the monofractal models. Indeed, from the point of view of multifractals, it would have been a miracle if for each threshold T, each (different) set had exactly the same fractal dimension.

It is worth mentioning that the functional box-counting results have impor-

tant consequences for classical geostatistics (e.g. [*Matheron*, 1970]) which assume (explicitly or implicitly) that geomeasures such as the areas of the topography exceeding a threshold are regular with respect to Lebesgue measures. If this assumption were true, then the areas above a given threshold T would be well-defined independently of the resolution L, i.e. the expression $L^2 N_T(L)$ would be independent of L; however since $D(T) < 2$ we see that generally it vanishes as $L \to 0$. Ultimately at millimetric or small scales, the scaling will break down yielding a finite limit of $L^2 N_T(L)$. However this value will depend on the very small scale details; at any larger resolutions the result will be subjective depending on the observing resolution L.

If we express the field values as powers of the resolution with random exponents γ, i.e. if we write $T \propto \lambda^\gamma$ then we obtain:

$$\Pr\left(\varepsilon_\lambda > T\right) = \Pr\left(\varepsilon_\lambda > \lambda^\gamma\right) \propto \lambda^{-c(\gamma)} \qquad (4)$$
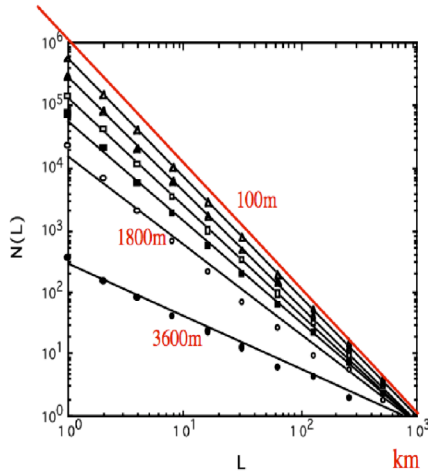

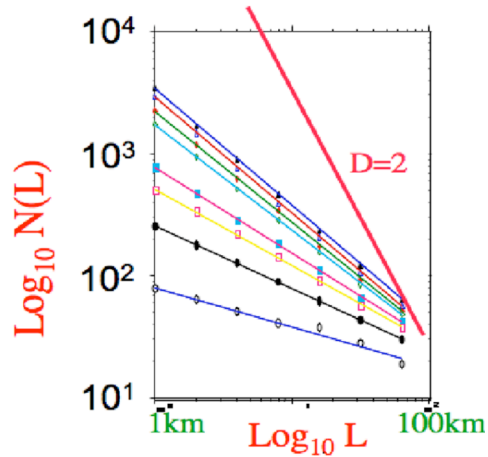| Fig. 4: Functional box-counting on French topography data at 1km resolution. For each threshold, the scaling is quite accurate, but as the threshold increases, the slope systematically decreases so that the topography is apparently not monofractal. The line with slope -2 is shown since this is the theoretical assumption of classical geostatistics. Adapted from [*Lovejoy and Schertzer*, 1990]. | Fig. 5: Functional box-counting on radar reflectivity data of rain; the data taken from a weather radar in Montreal, Canada. Each line corresponds to a reflectivity factor increasing by a factor of about 2.5 (starting at the top which is the lowest detectable signal). Although all the different levels are accurately power laws (scaling), the more and more intense rain regions (lower curves) have lower and lower slopes, again we conclude that rain is multifractal. Again, the geostatics theory slope 2 is shown for reference. Adapted from [*Lovejoy, et al.*, 1987]. |

where "Pr" indicates "probability". Since the moments (eq. 2) are integrals over the probability density (dPr), $c(\gamma)$ determines $K(q)$; indeed, the relationship can generally be inverted; we obtain the simple Legendre relation:

$$\left\{ c(\gamma) = \max_{q}\left(q\gamma - K(q)\right); \quad K(q) = \max_{\gamma}\left(q\gamma - c(\gamma)\right)\right\} \tag{5}$$

showing that there is a one-to-one relation between the orders of moments q, and orders of singularity γ and between $c(\gamma)$, $K(q)$ [*Parisi and Frisch*, 1985].

5. Cascades and data analyses

The nonlinear terms in the Navier-Stokes equations ruling 3D turbulence conserve the scale by scale (fourier) flux of energy from large to small scales. In addition, structures interact most strongly with other structures of nearly similar size. Finally, over a wide range, there is no characteristic scale in the nonlinear mechanism. This fourier conservation, fourier "locality" and scale invariance imply a cascade phenomenology, the basis for phenomenological cascades models. Starting with [*Novikov and Stewart*, 1964] [*Yaglom*, 1966, *Mandelbrot*, 1974] these models were developed to study the effects of intermittency. They start with an initially uniform large scale which is successively subdivided into smaller and smaller sub-structures, each multiplicatively modulating the energy flux from the larger scales, with the process repeating scale after scale until in turbulence, viscosity eventually cuts off the cascade (for the atmosphere, at millimetres). The resulting cascades have fluxes which respect eq. 2.

In order to empirically test this cascade prediction we may attempt to "invert" the cascade by successively degrading the resolution of the cascade quantities. The only complication is that observable quantities such as the turbulent velocity or the topographic altitude are generally *not* conserved scale by scale. For example in Kolmogorov turbulence, the velocity gradient Δv is related to the conserved energy flux ($\varepsilon_{\Delta x}$) at resolution Δx by:

$$\Delta v = \varepsilon_{\Delta x}^{a} \Delta x^{H}; \quad a = 1/3; \quad H = 1/3 \tag{6}$$

The usual interpretation of this formula (which is essentially the result of dimensional analysis), is that it expresses the equality of the scaling of the left and right hand sides of the equations, hence, averaging the qth power of eq. 6.:

$$\left\langle |\Delta v|^{q} \right\rangle = \left\langle \varepsilon_{\Delta x}^{qa} \right\rangle \Delta x^{qH} = \Delta x^{\xi(q)}; \quad \xi(q) = qH - K(qa) \tag{7}$$

where "<.>" means statistical averaging, and $\xi(q)$ is the (generalized) "q^{th} order structure function exponent". We see that to determine the $K(q)$ exponent characterizing the flux, we must either remove the Δx^{H} term in eq. 6 to

estimate ε^a, or we may use the structure function to directly determine $\xi(q)$ from eq. 7 and then remove the linear contribution qH. Since power law filtering of ε^a by k^{-H} in fourier space has the effect of introducing the linear scaling term Δx^H (see section 8), this suggests that to obtain ε^a from Δv, that we invert the integration by fractionally differentiating by an order H. It turns out that it suffices to fractionally differentiate with order > H so that for H<1 (the usual case), a standard finite difference approximation (such as in 1-D taking the absolute differences at the finest resolution, or in 2-D taking the modulus of the finite difference gradient vector), is adequate [*Lavallée, et al.*, 1993]. Figs, 6, 7, show the results on global atmospheric and topographic data. We see clearly that eq. 2 is accurately obeyed over the entire available ranges of scale, and that the effective outer scale (i.e. the scale where the cascade must have started if it is the only source of variability), is of the order of planetary scale (and in fig. 6 slightly larger indicating that there are other sources of variability at this scale). The figures show that the variability of both the weak (low q) and strong (high q) fluctuations at all the observed scales can be accurately accounted for by multiplicative cascade processes.

6. Multifractal Universality:

We have already mentioned that the generic result of cascade processes is that the conserved flux obeys eq. 2; i.e. it involves the convex function K(q). At this level the theory effectively involves an infinite number of parameters ($K(q)$). If no simplifications were to occur, this would be unmanageable. However, as is usually the case in physics when processes are sufficiently iterated or when interactions are sufficiently numerous, we expect that only some of the details will be important. This is the general problem of "universality"; for cascades the issue is complicated because of the highly singular small scale limit (see section 7). It is therefore important to consider the issue of universality over a fixed, (finite) range of scales, and only then take the small scale limit (see the debate [*Schertzer and Lovejoy*, 1997], and [*She and Levesque*, 1994] for a weaker "Log-Poisson" universality), the result is a kind of "multiplicative central limit theorem" leading to:

$$K(q) = \frac{C_1}{\alpha - 1}\left(q^\alpha - q\right)$$ (8)
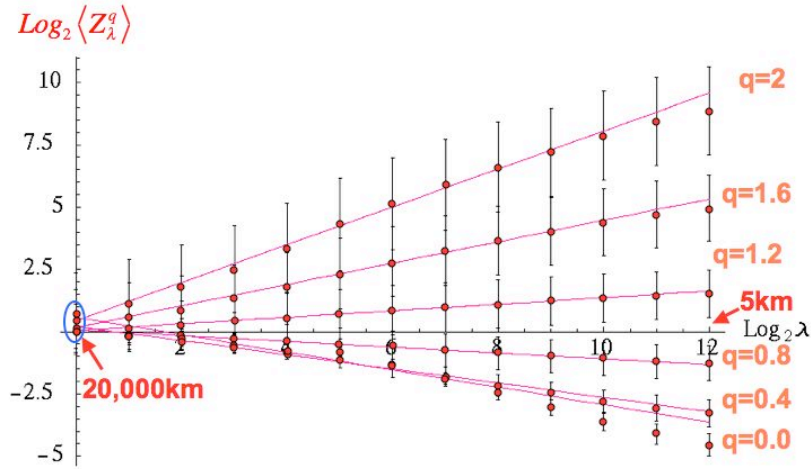
Fig. 6: Satellite radar reflectivities (Z) from the Tropical Rainfall Monitoring Mission (TRMM) covering the full planetary scale down to 5km. With the exception of very low order moment dominated by (nominally) zero rain reflectivity, the multiscaling holds remarkably well. The bars indicate the orbit to orbit variability, they are not errors. This figure uses data from the same local time of day, once every day, May 1-30, 2006, 250km swath, TRMM data (30 orbits). Analysis shows that $K(q)$ satisfies the universal form (eq. 8) with α=1.5, C_1=0.63, but with rain detectable above instrumental noise having a fractal support of codimension C_s=0.41. Multifractal modelling shows that the slight curvature in the above for low q is well explained by this simple threshold detection model: the moments of order <2 are determined within 7% over the entire range 20,000-5km by the two parameters α, C_1, and a threshold equal to one half the mean reflectivity, and an "effective external scale" ≈40,000km.

where $0<\alpha\leq2$ is the Levy index, and $0<C_1<d$ is the codimension of the mean [*Schertzer and Lovejoy*, 1987]. This can be roughly understood by taking the logs of the cascade which is the sum of a large number of logarithmic contributions and therefore (if appropriately centred, normalized) is subject to the additive central limit theorem (which is in fact one of the original applications of "universality" well before the idea became a generally recognized physics principle). The special case α=2 corresponds to "log-normal" cascades [*Kolmogorov*, 1962], the special case α=0 to the monofractal "β model" [*Frisch, et al.*, 1978]. Many atmospheric and terrestrial surface fields have now been shown to be compatible with eq. 8, and the universality parameters H, C_1, α have been estimated for several dozen geofields (for a review, see [*Lovejoy and Schertzer*, 1995]).
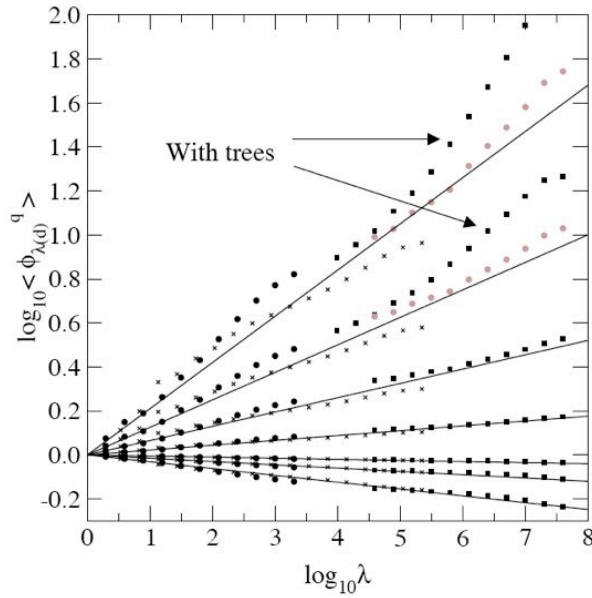
Fig. 7: Log/log plot of the normalized trace moments versus the scale ratio λ = *Louter/l* (with *Louter* = 20 000 km) for the three DEMs used in fig. 2 (circles correspond to ETOPO5, X's to U.S. and squares to Lower Saxony). The solid lines are there to distinguish between each value of q (from top to bottom, q=2.18, 1.77, 1.44, 1.17, 0.04, 0.12 and 0.51). The moments of the Lower Saxony DEM with trees for q=1.77 and q=2.18 are on the graph (indicated by arrows). The theoretical lines are computed with the global $K(q)$ function i.e. with α=1.79, C_1=0.12, for the parameter estimation and figure, reproduced from [*Gagnon, et al.*, 2006].

7. Multifractals, extremes and SOC; the multifractal Butterfly effect:

We have mentioned the huge impact of [*Bak, et al.*, 1987]'s paper linking apparently simple avalanche like "sandpile" models to extreme events with algebraic probability distributions. This "classical SOC" has spawned a large number of variants which exploit a cellular-automaton framework with a simple threshold rule applied at a small scale (grid) which leads to both fractal structures and algebraically distributed extremes. What is still underappreciated is the fact that multifractal cascade processes also generate fractal structures with algebraic probabilities: "nonclassical SOC". This effect - as in the usual (chaotic) butterfly effect - is the result of small scale disturbances dominating the large scale and has therefore been called the "multifractal butterfly effect" [*Lovejoy and Schertzer*, 1998b]. It's origin lies in the highly singular small scale cascade limit. This singular behaviour is particularly

wild in the general case where the cascade only respects "canonical" (scale by scale) conservation in which it is only the ensemble average energy flux which is conserved scale by scale [*Mandelbrot*, 1974]. In order to avoid the attendant technical difficulties, the simpler but much more restrictive "microcanonical conservation" is all too often considered but it does not have these strong extremes (e.g. the "p model", [*Meneveau and Sreenivasan*, 1987]). In the general canonical cascades, the small scale limit is only well-defined for integrals over finite sets; this leads to the distinction between "bare" cascades quantities (which are the result of the cascade developed over a given range of scales), and the "dressed" properties which are the result of the cascade developed down to infinitely small scales and then averaged up to the same scale. Below a critical order of moment q_D (which depends on the dimension of the averaging space, D), both the bare and dressed properties respect eq. 2; however, for $q>q_D$, the dressed moments (and hence $K(q)$) diverge whereas the "bare" moments converge (for all $q\geq0$). This implies:

$$\left\{ \langle \varepsilon_\lambda^q \rangle \to \infty; \quad q > q_D \right\} \Leftrightarrow \left\{ \Pr(\varepsilon_\lambda > s) \approx s^{-q_D}; \quad s \gg 1 \right\} \tag{9}$$

so that the dressed fluxes display the key feature of SOC: algebraic probabilities. This "nonclassical SOC" [*Schertzer and Lovejoy*, 1994] may often be physically more realistic than classical SOC since whereas the latter is only valid in the "zero-flux limit" (e.g. each sand grain must be added one by one only after the avalanches provoked by the preceding have ended), the multifractal SOC is a generic SOC mechanism valid in systems with quasi-constant fluxes. Note that moments are only infinite in the limit of infinite sample sizes. For a finite number of samples, we may have either first or second order "multifractal phase transitions" [*Schertzer, et al.*, 1993]. Fig. 8 shows that atmospheric turbulence is indeed apparently a SOC phenomenon. The extreme nature of multifractals is due to the fact that they can be viewed as random hierarchies of singularities (eq. 4); the structure of the extreme singularities can thus readily stand out. To study this it is helpful to make numerical simulations. Fig. 9 shows an example with a log-spiral singularity showing how cyclones can be modeled without needing special "cyclone" models, their "order" apparently emerging from chaos; in the next section we discuss simulations further.
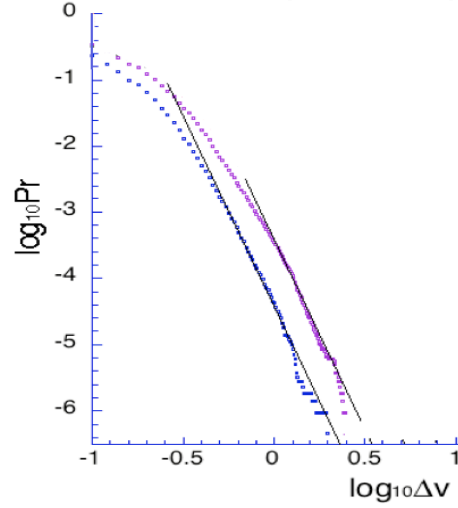
Fig. 8 This shows the probability distribution (cumulated from the largest to smallest) for horizontal velocity differences from the stratospheric ER2 aircraft. The horizontal gradients are given for distances of 40m, 80m (left, right), the reference slopes corresponds to eq. 9 with q_D=5.7 and. This value is in between the value 5 found in the vertical [*Schertzer and Lovejoy*, 1985a] and the temporal value q_D=7 (a surrogate for the horizontal, [*Schmitt, et al.*, 1994]). See also [*Tchiguirinskaia, et al.*, 2006], [*Tuck, et al.*, 2004]. The data are from 18 aircraft flights, each over paths 1000 -2000 km in length.

8. The Fractionally Integrated Flux model and Multifractal simulations:

To model scaling processes, it is natural to use combinations of scale invariant basis functions, i.e. mathematical singularities. Let's first consider the basic additive scaling process, fractional Brownian motion (fBm) and it's generalization, fractional Levy motion (fLm). These can be written as convolutions of noises with power laws i.e. fractional integrations:

$$v(\underline{x}) = \int \frac{\phi_\alpha(\underline{x}')d\underline{x}'}{|\underline{x}-\underline{x}'|^{D-H'}}; \quad H' = H + D/\alpha \tag{10}$$

ϕ_α is a Levy noise made of uncorrelated Levy random variables and H' is the order of fractional integration. Introducing the fluctuation $\Delta v(\Delta x) = v(x+\Delta x) - v(x)$, the resulting v field has statistics obeying:

$$\left\langle |\Delta v(\underline{\Delta x})|^q \right\rangle \approx |\underline{\Delta x}|^{\xi(q)}; \quad \xi(q) = qH \tag{11}$$

when $\alpha < 2$, $\xi(q)$ diverges for $q > \alpha$. These models are monofractal because the fractal codimension of any level set $v(\underline{x}) = T$ has a codimension $c(T) = H$ (i.e. independent of T).
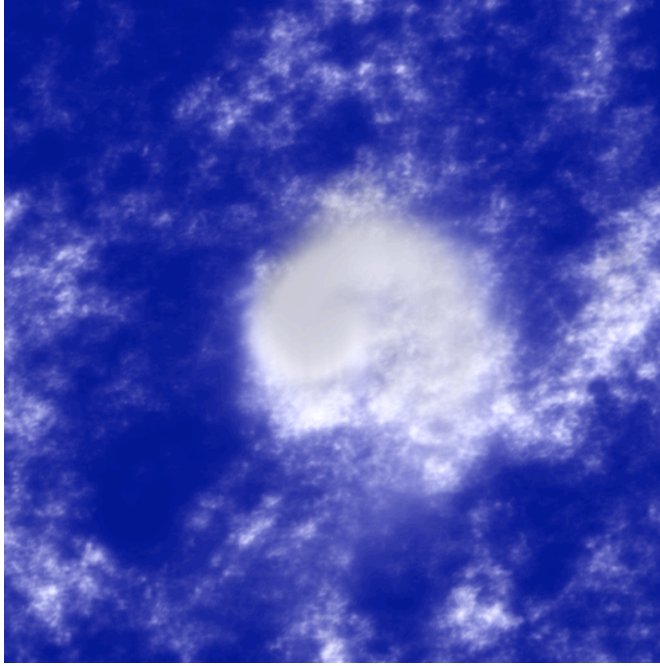
Fig. 9: A cyclone emerging from chaos. This multifractal simulation has roughly the observed universal multifractal parameters (α=1.8, C_1=0.1, H=0.33), but is symmetric with respect to a G with complex eigenvalues (hence structures rotate with scale). From time to time, the process produces particularly strong singularities which can dominate the simulation. Here, the event was sufficiently rare that it was "helped" by artificially increasing a single value of the 2^{24} elements of the subgenerator.

Fig. 10 shows a comparison of fBm, fLm and a universal multifractal process with the same H value. The multifractal process can also be modeled as a fractional integration of a noise, although this time, the noise is a conservative (cascade) multifractal (a "flux", hence the name Fractionally Integrated Flux, FIF model):

$$v_\lambda(\underline{x}) = \int \frac{\varepsilon_\lambda(\underline{x}')d\underline{x}'}{|\underline{x}-\underline{x}'|^{D-H}}; \quad \varepsilon_\lambda(\underline{x}') = e^{\Gamma_\lambda(\underline{x}')}; \quad \Gamma_\lambda(\underline{x}) \propto \int\limits_{1<|\underline{x}'|<\lambda} \frac{\phi_\alpha(\underline{x}')d\underline{x}'}{|\underline{x}-\underline{x}'|^{D-H'}} \tag{12}$$

where ϕ_α is a maximally skewed Levy noise process and $H'=D(1-1/\alpha)$. The resulting ε_λ is multiplicative because it is an exponentiation of the additive generator Γ_λ. From fig. 10 we can see that the fBm gives a relatively uninteresting texture. fBm is fairly limited in its possibilities since due to the central limit theorem (the gaussian special case), a process with the same statistical properties can be produced by using singularities of quite different shapes; it is insensitive to the shape. The fLm on the contrary has extremes

which are too strong; as one can see, several strong mountain peaks stand out; in fact, the strong peaks are too strong. Although far from Gaussian, real topography empirically seems to have finite variance (i.e. the probability density tail falls off faster than x^{-3}), so fLm is not a good model. Finally, the multifractal simulation has much more interesting structures, however we are missing the interesting ridges, valleys and other anisotropic features of real geomorphologies.
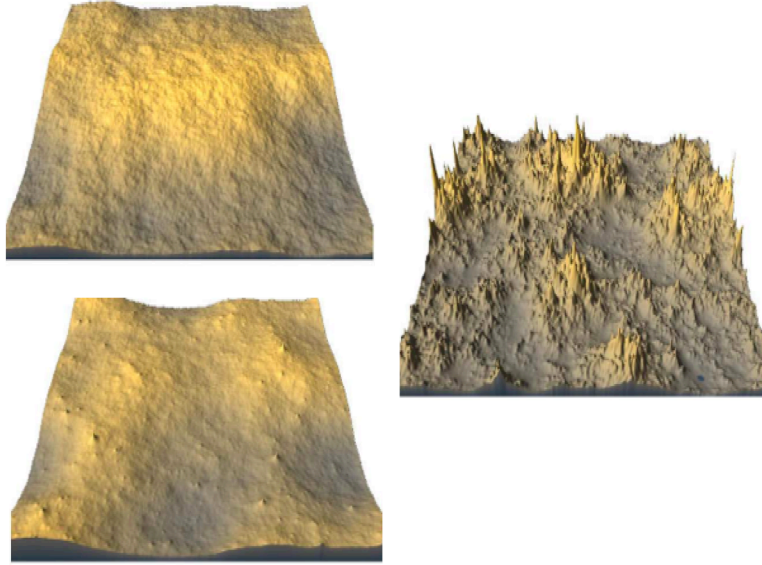

Fig. 10: The upper left simulation shows fBm, with H=0.7, lower left fLm with H=0.7, α =1.8, and the right the Multifractal FIF with H=0.7, α =1.8, C_1=0.12 (close to observations for topography, see [*Gagnon, et al.*, 2006]). For more examples of multifractal simulations, see the multifractal explorer site: http://www.physics.mcgill.ca/~gang/multifrac/index.htm.

Considering the "universal multifractals" v_λ, defined by eq. 12 we see that they are isotropic (the singularities have no preferred directions, they depend only on the vector norm), they are therefore "self-similar"; "zoomed" structures will (on average) resemble the unzoomed ones. In addition, they depend on three parameters: the H in eq. 12, and the α, C_1 which define the statistics of the generator Γ_λ. While the parameter H is the order of fractional integration and quantifies the degree of scale invariant smoothing, the qualitative effects of the codimension of the mean (C_1) and the Levy index (α) are less easy to see. We therefore performed multifractal simulations (fig. 11) which systematically show the morphologies of the structures obtained by varying these three parameters. The simulations use false colors and each

has the same initial random "seed" so that the basic structures are the same. For reference, note that the empirically most common values of α are in the range 1.5-1.8 (the latter being appropriate for topography and cloud radiances, the former, for rain and atmospheric turbulence). The parameter C_1 is often fairly low (e.g. in the range 0.05-0.15 for the wind, cloud radiances, topography), although it can be large (0.25-0.7) for rain and turbulent fluxes. While the basic Kolmogorov value of H is 1/3, many fields (such as cloud radiances) are near this, while rain is nearly zero, topography is in the range 0.45-0.7. From fig. 11 we can see that high values of C_1 lead to fields totally dominated by one or two strong structures, while low α values lead to fields dominated by "Levy holes": large regions with extremely low values.

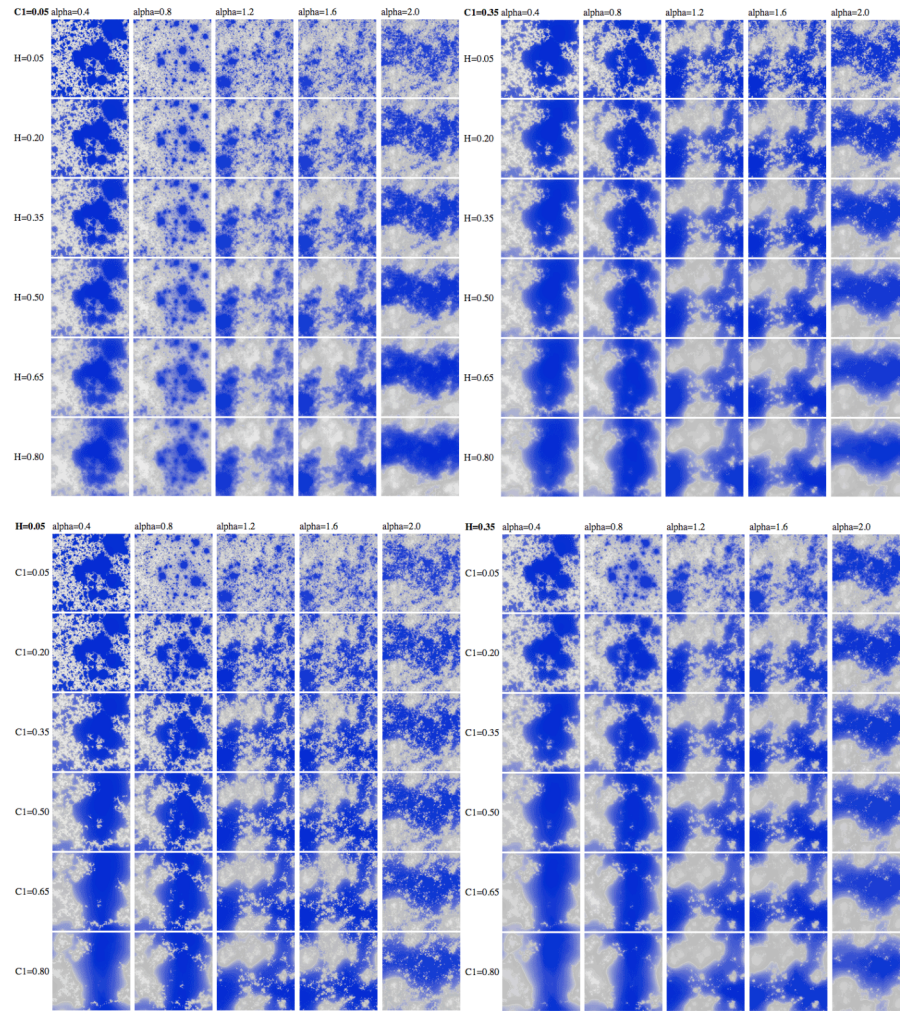Fig. 11: This shows the effect of varying α, C_1, H values on multifractal simulations. The upper figures show the effect of increasing α (left to right, 0.4, 0.8, …2.) and H (top to bottom 0.05, 0.2, …0.8) with C_1 fixed (=0.05 left, 0.35 right). The lower figures show the effect of varying α (left to right, 0.4, 0.8, …2.) and C_1 (top to bottom 0.05, 0.2, …0.8) with H fixed (=0.05 left, 0.35 right).

Fig. 12a: This self-affine simulation illustrates the "phenomenological fallacy" since both the top and bottom look quite different while having the same generators (*G* is diagonal with elements 0.8, 1.2), same (anisotropic) statistics at scales differing by a factor of 64 (top and bottom blow-up). The figure shows the proverbial geologists' lens cap at two resolutions differing by a factor of 64. Seen from afar (top), the structures seem to be composed of left to right ridges, however closer inspection (bottom) shows that in fact this is not the case at the smaller scales.

Fig. 12b: This shows a multifractal simulation looking horizontally through a horizontally stratified cloud layer with $\alpha=1.8$, $C_1=0.1$, $H=0.333$ of a stratified 3D cloud with G diagonal with elements 1, 5/9. This corresponds to a Kolmogorov scaling in the horizontal ($k^{-5/3}$) but a Bolgiano-Obukhov ($k^{-11/5}$) scaling in the vertical. Single scatter radiative transfer was used for the rendering.
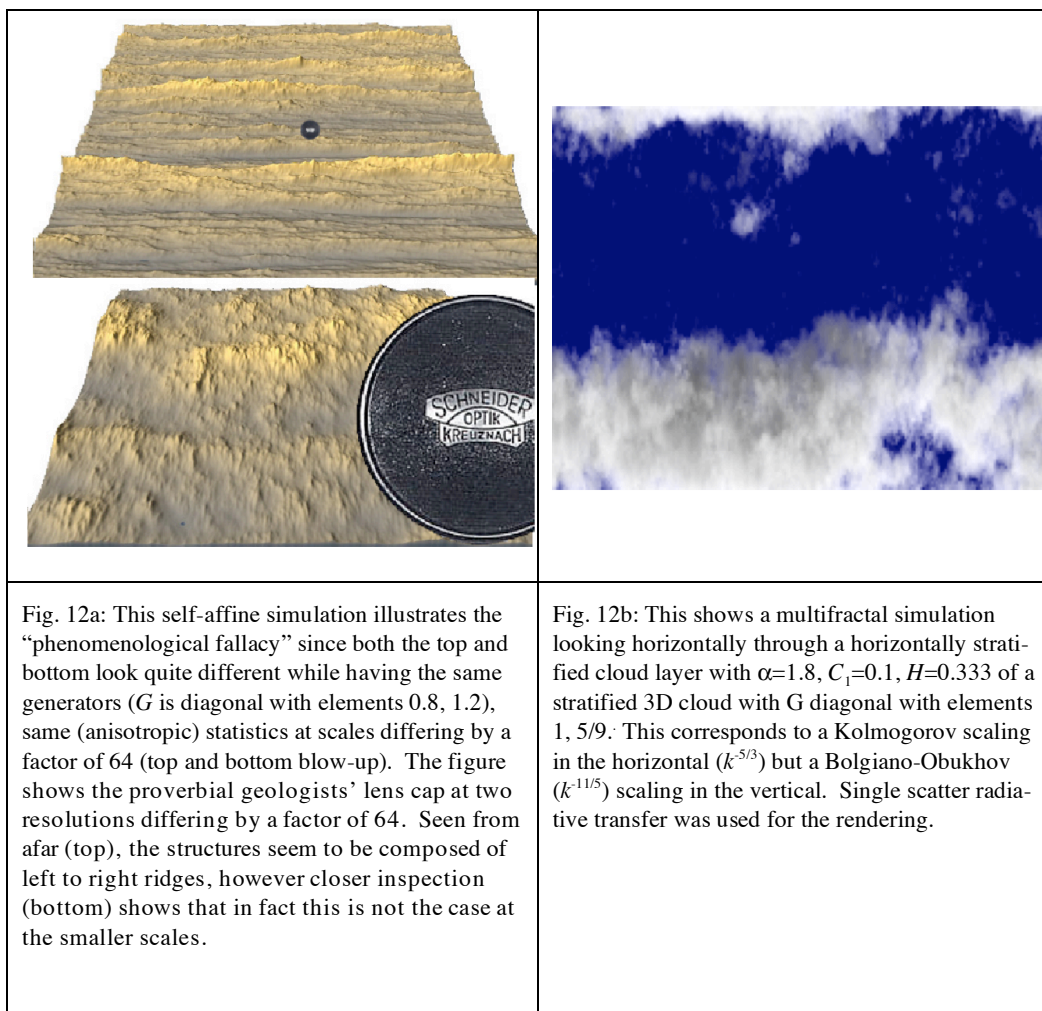
Fig. 13: A multifractal simulation of a 3D stratified cloud (with the same G as fig. 10b) with single scattered radiative transfer. Henyey-Greenstein phase functions were used with asymmetry factor g=0.85.

9. The phenenological fallacy and Generalized Scale Invariance:

Geophysicists commonly derive their models from phenomenological classifications based largely on classical (scale bound) notions of scale and shape. Once a phenomenon has been defined - often involving somewhat subjective criterion – models are constructed to explain them. However in this section we shall see that scaling processes – if based on sufficiently strong anisotropic singularities, can lead to quite different looking structures at different scales even though the basic mechanism is scale invariant; see fig. 12a for an example (and below for a more systematic survey). This possibility demonstrates what we call the "phenomological fallacy" i.e. the danger of inferring process from appearance.

In order to change the shape of the singularities while conserving the basic statistical properties of the process, it turns out to be sufficient to make the replacement everywhere eqs. 10-12:

$$|\underline{\Delta x}| \rightarrow \|\underline{\Delta x}\|; \quad D \rightarrow D_{el} \tag{13}$$

i.e. to replace the usual distance ("$|\ \ |$") by a "scale function" ("$\|\ \ \|$") and usual dimension of space by an "elliptical dimension" D_{el} which satisfies the following basic equation scaling:

$$\|T_\lambda \underline{x}\| = \lambda^{-1}\|\underline{x}\|; \quad T_\lambda = \lambda^{-G}; \quad D_{el} = TraceG \tag{14}$$

where T_λ is a scale changing operator which reduces the scale of a vector by a factor λ. In order for the scale function to be scaling (i.e. have no characteristic scale), it must satisfy group properties, hence it must admit a generator G as indicated.

Once all the unit vectors $\underline{x}_1$ are specified the nonunit vectors ($\|\underline{x}_\lambda\| = \lambda; \quad \lambda \neq 1$)

are then generated by the action of T_λ: $\underline{x}_\lambda = T_\lambda \underline{x}_1$; see [*Schertzer and Lovejoy*, 1985b] for technical details on this Generalized Scale Invariance, GSI. The set of all vectors $\|\underline{x}\| \leq \lambda$ is called a "ball", denoted B_λ; for physical scale functions B_λ must be strictly decreasing (i.e. $B_{\lambda'} \subseteq B_\lambda; \quad \lambda' < \lambda$). We can see that if the replacements $|\underline{x} - \underline{x}'| \rightarrow \|\underline{x} - \underline{x}'\|; \quad D \rightarrow D_{el}$ are made in the denominators of eqs. 10,

12, with scale functions satisfying eq. 14 then the convolutions will have power law dependencies under "zooming", i.e. the models will be scaling as long as the noises are also scaling (hence the special choices of Gaussian or Levy noise, or in the multifractal case, of multifractal noises).

To understand the relation between usual distances and generalized scales it is instructive to consider a simple scale function. Consider a (real) 2-D G matrix which we diagonalize to yield $G = \text{diag}(H_x, H_y)$ (note that what follows can be generalized to complex eigenvalues or nondiagonalizable matrices). We may now make the following nonlinear transformation:

$$\underline{x}' = (x', y') = \left(\text{sgn}(x)|x|^{1/H_x}, \text{sgn}(y)|y|^{1/H_y} \right) \tag{15}$$

It is then easy to verify that $\|\lambda^{-1}\underline{x}'\| = \lambda^{-1}\|\underline{x}'\|$ i.e. $\underline{x}$' satisfies the scale eq. 14 but with $G = I =$ the identity corresponding to the generator of an isotropic scale transformation. When $G = I$ it is easy to verify that a family of solutions of the scale function eq. 14 is:

$$\|\underline{x}'\| = \Theta(\theta')r' \tag{16}$$

where (r', θ') are polar coordinates:

$$r' = |\underline{x}'| = \left(x^{2/H_x} + y^{2/H_y} \right)^{1/2}; \quad \tan\theta' = \frac{y'}{x'} = \frac{\text{sgn}(y)|y|^{1/H_y}}{\text{sgn}(x)|x|^{1/H_x}} \tag{17}$$

and Θ is an arbitrary positive function which specifies the shape of the unit ball (i.e. those vectors with $\|\underline{x}'\| = 1$; their polar equation is r'$=1/\Theta(\theta')$) it determines the "trivial" anisotropy (the nonscaling part).

When scale functions are used as the basic singularities, the shapes can be extremely varied, hence demonstrating the possibility of modeling geomorphologies in this way. First consider $G = I$: the resulting models will be

"self-similar" in the sense that their statistics will vary in power law ways under isotropic "zooming" (blow-ups). If G is a diagonal matrix, then the singularities $\|x\|^{-\gamma}$ (where γ is the order of singularity, see eq. 4) are quite different in different directions and the resulting fractals/multifractals are "self-affine" (fig. 12 and 14a bottom row). The case where G is nondiagonal and the eigenvalues are real is a generalization in which the main stretching/shrinking occurs along fixed nonorthogonal eigendirections (see fig. 12, 14). When the eigenvalues are complex, the eigenvectors rotate continuously as functions of scale, giving rise to spiral type singularities, see fig. 9.

In order to systematically see the effect of varying G, we can parametrize it as follows:

$$G = \begin{pmatrix} d-c & f-e \\ f+e & d+c \end{pmatrix} \tag{18}$$

Defining $a^2 = c^2 + f^2 - e^2$ we see that G has eigenvalues $d+a$, $d-a$, As indicated above, real a is "stratification dominant" (structures rotate no more than once with scale) whereas imaginary a is "rotation dominant" structures rotate an infinite number of times with scale. In order to explore the parameter space, we note that there are 3 rotational invariants: d, a, $(f^2+c^2)^{1/2}$. Hence for example, taking $f=0$, and varying c loses no generality (other f values are obtained by rotation). Also, we can fix $d=1$ since it turns out that we can always replace G by G/d as long as we compensate by simultaneously taking the d power of the scale function) i.e we lose no generality with $d=1$. The two G parameters we explore are thus c, e. The use of a final parameter k allows us to examine the effect of possibly very nonroundish unit scales (see eq. 16). We define it as:

$$\Theta(\theta') = 1 + \frac{1-2^{-k}}{1+2^{-k}}\cos\theta' \tag{19}$$

With this definition, we see that $k= \log_2 (r'_{max}/r'_{min})$ where r'_{max}, r'_{min} are the maximum and minimum radii of the sphero-scale (in the r' space, but this will be close to the ratio in the r space). $k=10$ thus corresponds to a unit scale which "mixes" conventional scales over a factor of more than 1000 (2^{10}).

The effect of varying the parameters c, e, k is shown in the multifractal simulations shown in fig. 14. All the simulations have $\alpha=1.8$, $C_1=0.1$, $H=0.33$ (the empirical parameters for clouds), and are simulated on 256X256 grids with the same starting seed so that the differences are only due to the anisotropy (the colours go from blue to white indicating values low to high). For isotropic unit scales ($k=0$, top row fig. 14a) we see the effect of varying c. On the right we display the contours of the corresponding scale functions.
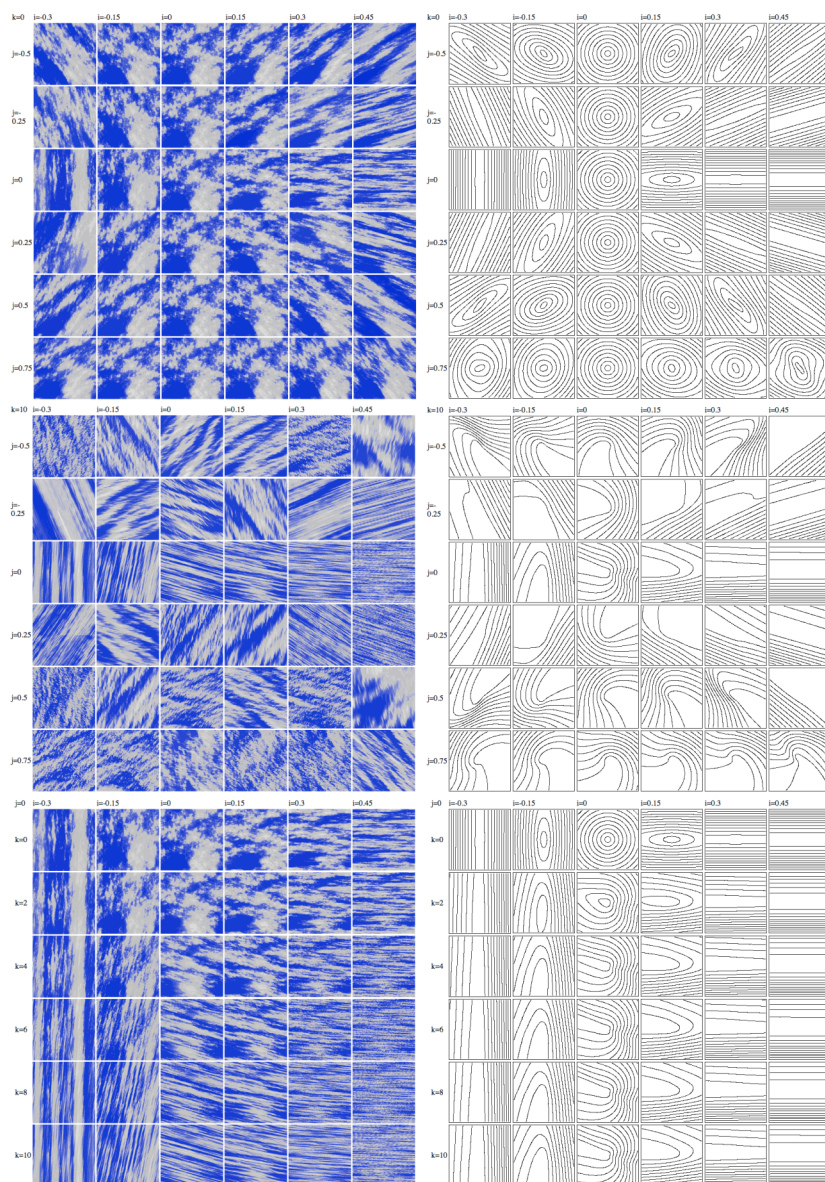
Fig. 14a: <u>Top row</u>: *k*=0,we vary *c* (denoted *i*) from -0.3, -0.15, …0.45 left to right and *e* (denoted *j*) from -0.5, -0.25, …0.75 top to bottom. On the right we show the contours of the corresponding scale functions. <u>Middle row</u>: Same except that *k*=10. <u>Bottom row</u>: *e*=0 the *c* is increased from -0.3, -0.15, …0.45 left to right, from top to bottom, *k* is increased from 0,2,4,..10. See text for more details.
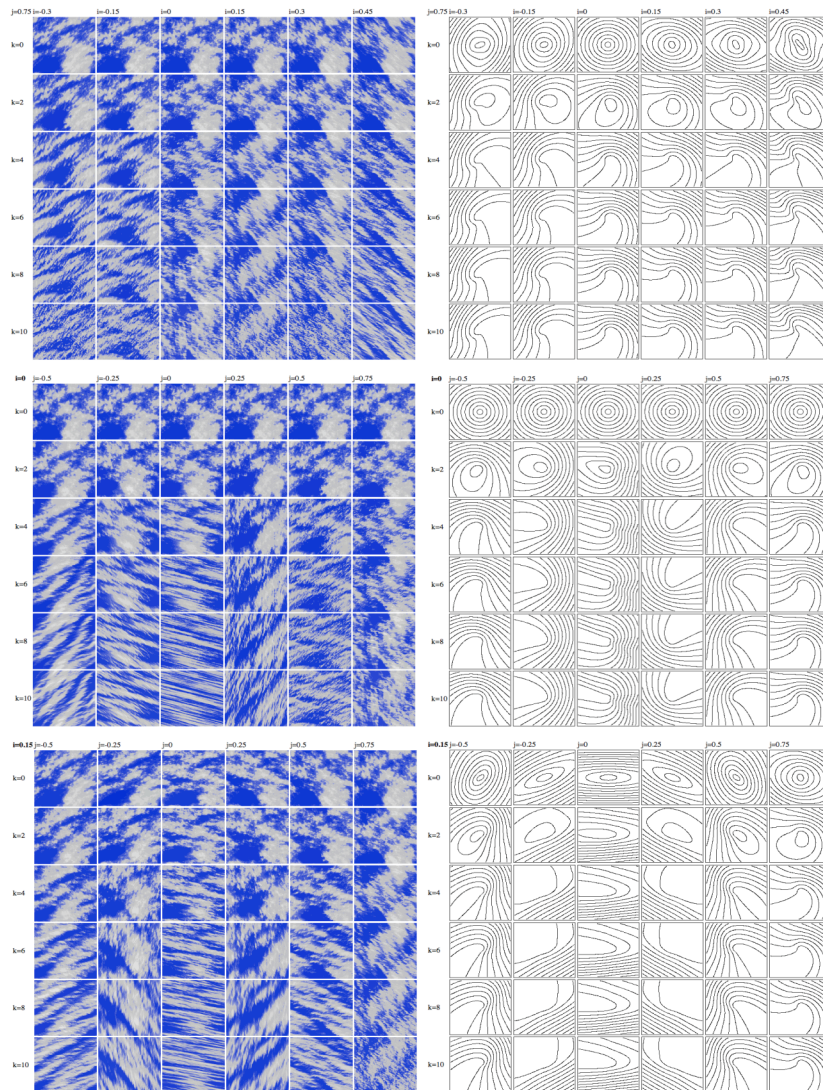
Fig. 14b: <u>Top row</u>: The same as the bottom row of 13a except that *e* =0.75. <u>Middle row</u>: *c*=0 and *e* left to right is: -0.5, -0.25, …0.75. <u>Bottom row</u>: Same as the middle row except that *c*=0.15. In all rows, from top to bottom, *k* is increased (0,2,4,..10), the right hand shows the corresponding scale functions.

Moving down to the middle row we take *k*=10 so that the unit ball has a range of scales of 2^{10}; the structures are more filamentary. In the bottom row

we take $e=0$ displaying the effect of varying c: G is thus diagonal, the structures are "self-affine" (no rotation). Fig. 14b (top row) is the same as the bottom row of fig. 14a except that $e =0.75$ showing the effect of rotation. Since $a^2=c^2-e^2<0$ here ($f=0$), the eigenvectors of λ^{-G} rotate continuously with scale. In the middle row we fix $c=0$ and vary e, the bottom row is the same except that $c=0.15$ so that there is both the effect of stratification (c), and rotation (e). Here the eigenvalues are again complex except in the third column with $e=0$.Finally, outside our present scope but presumably important for realistic geophysical modeling, we can consider G as a nonlinear operator (rather than a matrix). In this case, the anisotropy depends not only on scale but also on the location. This allows for spatially varying morphologies. In this case, the linear GSI discussed above is simply a locally valid approximation. In this case, the anisotropy depends not only on scale but also on the location. This allows for spatially varying morphologies. In this case, the linear GSI discussed above is simply a locally valid approximation.

10. Conclusions:

We are all aware of the extreme variability of geophysical fields over huge ranges of scales: the atmosphere has structures as small as millimeters, and as large as the planet; a ratio of 10^{10}; the surface topography apparently has an even larger ratio. The mathematical modelling of this variability has long stimulated mathematicians and physicists. For example [*Perrin*, 1913] considered the problem of differentiability: "Consider the difficulty in finding the tangent to a point of the coast of Brittany... depending on the resolution of the map the tangent would change. The point is that a map is simply a conventional drawing in which each line has a tangent. On the contrary, an essential feature of the coast is that ... without making them out, at each scale we *guess* the details which prohibit us from drawing a tangent...". The converse problem - integrability ("rectifiability") was considered by [*Steinhaus*, 1954] "... The left bank of the Vistula when measured with increased precision would furnish lengths ten, hundred, and even a thousand times as great as the length read off a school map. A statement nearly adequate to reality would be to call most arcs encountered in nature as not rectifiable. This statement is contrary to the belief that not rectifiable arcs are an invention of mathematicians and that natural arcs are rectifiable: it is the opposite which is true...". [*Richardson*, 1961] quantified integrability by considering the empirical scaling of the coast of Britain and of several frontiers using the "Richardson dividers" method. In his paper [*Mandelbrot*, 1967] "How long is the coast of Britain?" Richardson's scaling exponent was interpreted in

terms of a fractal dimension. Later, in his seminal "Fractals: form, chance and dimension" [*Mandelbrot*, 1977] proposed that fractals are ubiquitous in nature. However, when it came to geophysical applications although stimulating, this audacious idea was disappointing: most geofields of interest were mathematical fields (i.e. with a value at each space-time point such as the atmospheric temperature), and cannot be reduced to geometric sets of points. Furthermore, at that time, the proposed fractal sets were only scale invariant under isotropic scale changes (or occasionally the slightly more general self-affine scale changes in which different exponents act in different orthogonal directions). In a number of fields, by the early 1990's this restrictive isotropic monofractal framework was found to be quite inadequate leading in at least one instance - earth surface morphology – to the virtual abandonment of scaling approaches.

In this paper we argued that the key to understanding systems with large numbers of freedom with nonlinear dynamics acting over wide scale ranges was to generalize the notion of scale invariance (and indeed, of scale) in the framework of Generalized Scale Invariance and the basic mathematical object from fractal sets to multifractal functions (or more precisely, densities of measures). While the motivation of the former was to allow the nonlinear dynamics of the system to define the appropriate notion of scale (rather than to impose a priori isotropic, Euclidean notions), the motivation for the latter was to handle nonlinear processes which repeat scale after scale, the generic multifractal process being the cascade.

However, cascades have nontrivial, nonclassical properties, one of them being their highly singular small scale limit which leads to the distinction between "bare" and "dressed" cascade quantities. While the former is the result of the cascade developed from a large scale down to a given (finite) scale, and involves only the larger scale interactions – the latter is the result of integrating ("dressing") a fully developed cascade to the same scale. While the former has long-tailed statistics (e.g. log-Levy, log normal), the latter has fat, "algebraic" tails. If we adopt an operational definition of Self-Organized Criticality as a system with fractal structures and with strong algebraic distributions of extremes, then multifractals generically provide a nonclassical route to SOC.

As seductive as they are, multifractals involve an infinite hierarchy of exponents, and hence would be useless without some simplifying principle. Fortunately, stable, attractive universality classes exist with only three parameters, this enables both compact parametrisations of the exponent functions (and hence the empirical characterization of scaling geofields), it also allows for numerical simulations. In the last part of this paper we show how to make numerical simulations of clouds and topography which are quite realistic both statistically and visually.

During the last twenty years, we have seen the transition from fractal geometry to multifractal processes; we have seen how extremes can be tamed with the help of Self-Organized Criticality, we have witnessed the opening of new areas of applications by generalizing scale invariance from isotropic to anisotropic systems. These developments have in turn paved the way for systematic empirical characterizations of both solid earth and atmospheric geofields, they help overcome longstanding measurement problems (such as the interpretation of aircraft data). They have created the framework needed for realistic modeling of geofields over potentially huge ranges of scale.

11. Acknowledgements:

12. References:

Bak, P., et al. (1987), Self-Organized Criticality: An explanation of 1/f noise, *Physical Review Letter*, *59*, 381-384.

Dewan, E. (1997), Saturated-cascade similtude theory of gravity wave sepctra, *J. Geophys. Res.*, *102*, 29799-29817.

Feigenbaum, M. J. (1978), Quantitative universality for a class of nonlinear transformations, *J. Stat. Phys.*, *19*, 25.

Frisch, U., et al. (1978), A simple dynamical model of intermittency in fully develop turbulence, *Journal of Fluid Mechanics*, *87*, 719-724.

Gagnon, J., S., et al. (2006), Multifractal earth topography, *Nonlin. Proc. Geophys.*, *13*, 541-570.

Gardner, C. (1994), Diffusive filtering theory of gravity wave spectra in the atmosphere, *J. Geophys. Res.*, *99*, 20601.

Klinkenberg, B., and M. F. Goodchild (1992), The fractal properties of topography: A comparison of methods, *Earth surface Proc. and Landforms*, *17*, 217-234.

Kolesnikov, V. N., and A. S. Monin (1965), Spectra of meteorological field fluctuations, *Izvestiya, Atmospheric and Oceanic Physics*, *1*, 653-669.

Kolmogorov, A. N. (1962), A refinement of previous hypotheses concerning the local structure of turbulence in viscous incompressible fluid at high Raynolds number, *Journal of Fluid Mechanics*, *83*, 349.

Lavallée, D., et al. (1993), Nonlinear variability and landscape topography: analysis and simulation, in *Fractals in geography*, edited by L. De Cola and N. Lam, pp. 171-205, Prentice-Hall, Englewood, N.J.

Lilley, M., et al. (2004), 23/9 dimensional anisotropic scaling of passive admixtures using lidar aerosol data, *Phys. Rev. E*, *70*, 036307-036301-036307.

Lindborg, E., and J. Cho (2001), Horizontal velocity structure functions in the upper troposphere and lower stratosphere i-ii. Observations, theoretical considerations, *J. Geophys. Res.*, *106*, 10223.

Lorenz, E. N. (1963), Deterministic Nonperiodic flow, *J. Atmos. Sci.*, *20*, 130-141.

Lovejoy, S., and D. Schertzer (1986), Scale invariance in climatological temperatures and the

spectral plateau, *Annales Geophysicae*, *4B*, 401-410.

Lovejoy, S., and D. Schertzer (1990), Our multifractal atmosphere: A unique laboratory for non-linear dynamics, *Physics in Canada*, *46*, 62.

Lovejoy, S., and D. Schertzer (1995), How bright is the coast of Brittany? in *Fractals in Geoscience and Remote Sensing*, edited by G. Wilkinson, pp. 102-151, Office for Official Publications of the European Communities, Luxembourg.

Lovejoy, S., and D. Schertzer (1998a), Stochastic chaos and multifractal geophysics, in *Chaos, Fractals and models 96*, edited by F. M. Guindani and G. Salvadori, Italian University Press.

Lovejoy, S., and D. Schertzer (1998b), Stochastic chaos, scale invariance, multifractals and our turbulent atmosphere, in *ECO-TEC: Architecture of the In-between*, edited by e. b. A. Marras, p. in press, Storefront Book series, copublished with Princeton Architectural Press.

Lovejoy, S., and D. Schertzer (2005), Multifractals, cloud radiances and rain, *J. Hydrol.*, *Doi:10.1016/j.hydrol.2005.02.042*.

Lovejoy, S., et al. (1987), Functional Box-Counting and Multiple Dimensions in rain, *Science*, *235*, 1036-1038.

Lovejoy, S., et al. (2004), Fractal aircraft trajectories and nonclassical turbulent exponents, *Physical Review E*, *70*, 036306-036301-036305.

Lovejoy, S., et al. (2006), Is Kolmogorov turbulence relevant in the atmosphere? *Nature Physics*, *(submitted)*.

Mandelbrot, B. B. (1967), How long is the coastline of Britain? Statistical self-similarity and fractional dimension, *Science*, *155*, 636-638.

Mandelbrot, B. B. (1974), Intermittent turbulence in self-similar cascades: divergence of high moments and dimension of the carrier, *Journal of Fluid Mechanics*, *62*, 331-350.

Mandelbrot, B. B. (1977), *Fractals, form, chance and dimension*, Freeman, San Francisco.

Matheron, G. (1970), Random functions and their applications in geology, in *Geostatistics*, edited by D. F. Merriam, pp. 79-87, Plenum Press, New York.

Meneveau, C., and K. R. Sreenivasan (1987), Simple multifractal cascade model for fully develop turbulence, *Physical Review Letter*, *59*, 1424-1427.

Nastrom, G. D., and K. S. Gage (1983), A first look at wave number spectra from GASP data, *Tellus*, *35*, 383.

Novikov, E. A., and R. Stewart (1964), Intermittency of turbulence and spectrum of fluctuations in energy-disspation, *Izv. Akad. Nauk. SSSR. Ser. Geofiz.*, *3*, 408-412.

Parisi, G., and U. Frisch (1985), A multifractal model of intermittency, in *Turbulence and predictability in geophysical fluid dynamics and climate dynamics*, edited by M. Ghil, et al., pp. 84-88, North Holland, Amsterdam.

Perrin, J. (1913), *Les Atomes*, NRF-Gallimard, Paris.

Richardson, L. F. (1961), The problem of contiguity: an appendix of statistics of deadly quarrels, *General Systems Yearbook*, *6*, 139-187.

Rodriguez-Iturbe, I., and A. Rinaldo (1997), *Fractal River Basins*, 547 pp., Cambridge University Press, Cambridge.

Sachs, D., et al. (2002), The multifractal scaling of cloud radiances from 1m to 1km, *Fractals*, *10*, 253-265.

Schertzer, D., and S. Lovejoy (1985a), The dimension and intermittency of atmospheric dynamics, in *Turbulent Shear Flow 4*, edited by B. Launder, pp. 7-33, Springer-Verlag.

Schertzer, D., and S. Lovejoy (1985b), Generalised scale invariance in turbulent phenomena, *Physico-Chemical Hydrodynamics Journal*, *6*, 623-635.

Schertzer, D., and S. Lovejoy (1987), Physical modeling and Analysis of Rain and Clouds by Anisotropic Scaling of Multiplicative Processes, *Journal of Geophysical Research*, *92*, 9693-9714.

Schertzer, D., and S. Lovejoy (1994), Multifractal Generation of Self-Organized Criticality, in *Fractals In the natural and applied sciences*, edited by M. M. Novak, pp. 325-339, Elsevier,

North-Holland.

Schertzer, D., and S. Lovejoy (1997), Universal Multifractals do Exist! *J. Appl. Meteor.*, *36*, 1296-1303.

Schertzer, D., et al. (1993), Generic Multifractal phase transitions and self-organized criticality, in *Cellular Automata: prospects in astronomy and astrophysics*, edited by J. M. Perdang and A. Lejeune, pp. 216-227, World Scientific.

Schertzer, D., et al. (2002), Which chaos in the rainfall-runoff process? *Hydrol. Sci.*, *47*, 139-148.

Schmitt, F., et al. (1995), Multifractal analysis of the Greenland Ice-core project climate data., *Geophys. Res. Lett*, *22*, 1689-1692.

Schmitt, F., et al. (1994), Empirical study of multifractal phase transitions in atmospheric turbulence, *Nonlinear Processes in Geophysics*, *1*, 95-104.

She, Z., S., and E. Levesque (1994), *Phys. Rev. Lett.*, *72*, 336.

Steinhaus, H. (1954), Length, Shape and Area, *Colloquium Mathematicum*, *III*, 1-13.

Tchiguirinskaia, I., et al. (2006), Wind extremes and scales: multifractal insights and empirical evidence, in *EUROMECH Colloquium on Wind Energy*, edited by P. S. Eds. J. Peinke, Springer-Verlag.

Tuck, A. F., et al. (2004), Scale Invariance in jet streams: ER-2 data around the lower-stratospheric polar night vortex, *Q. J. R. Meteorol. Soc.*, *130*, 2423-2444.

Van der Hoven, I. (1957), Power spectrum of horizontal wind speed in the frequency range from.0007 to 900 cycles per hour, *Journal of Meteorology*, *14*, 160-164.

Yaglom, A. M. (1966), The influence on the fluctuation in energy dissipation on the shape of turbulent characteristics in the inertial interval, *Sov. Phys. Dokl.*, *2*, 26-30.